ACS OMEGA

Open Access

http://pubs.acs.org/journal/acsodf

Article

Research upon Cu-Doping Contents in TiO_2 Nanoparticles Incorporated onto Cellulose Nanofibers for Dye Removal and Self-Cleaning Applications

Duy-Nam Phan,* Thi Ngat Tran, Phuong-Linh Nguyen, Minh Thang Le, Azeem Ullah, and Ick-Soo Kim*

Cite This: *ACS Omega* 2024, 9, 22734−22743

Read Online

ACCESS | Metrics & More | Article Recommendations

ABSTRACT: Cu-doping contents in the TiO_2 lattice structure were studied to show the effects on the crystal structure, morphology, and photocatalytic activity of TiO_2 nanoparticles and thus composite cellulosic nanofibrous membranes. Pristine and copper-doped TiO_2 nanoparticles were synthesized using the sol−gel technique, a wet chemical method with the advantages of low synthesizing temperature, uniform nanosize distribution, and purity. The as-synthesized semiconductor nanoparticles were first tested with the dye removal process and then impregnated onto electrospun cellulose nanofibers (CL nanofibers) to acquire modified nanofibers with self-cleaning properties. The as-prepared composite CL nanofibers consisting of doped and undoped TiO_2 nanoparticles were characterized by various techniques, such as field emission scanning electron microscopy, transmission electron microscopy, UV−vis, X-ray diffraction, Fourier transform infrared spectroscopy, and tensile tests. The copper-doped TiO_2 molar ratio in the nanocomposite was found to possess a pronounced impact on the dye removal and self-cleaning effects under the visible light spectrum, whereas TiO_2 is highly effective under specific UV-light irradiation. Optical measurements and dye decomposition showed that the Cu-doped TiO_2 nanocomposite was optimized at a 1% molar ratio by the copper-doping concentration regarding dye removal and self-cleaning applications under the visible light range.

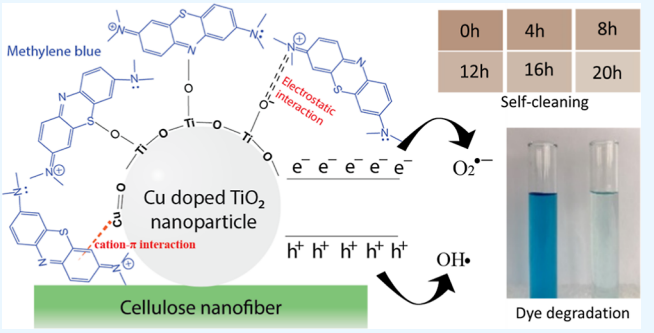

INTRODUCTION

TiO_2 has been extensively studied and proved to be one of the most efficient and widely used photocatalysts for varied applications including organic compound degradation with many advantages such as low production cost, high stability in acidic, alkaline, solvents, and good photocatalytic activity. The band gap energy values of two most-encountered phases of TiO_2 are rutile and anatase having energy band gaps of 3.0 and 3.2 eV,[1] respectively, which require UV rays having smaller than 410 nm radiation wavelength. Therefore, pristine TiO_2 has low photocatalytic performance under normal lighting conditions such as sunlight and fluorescent lights, which are visible regions of the spectrum. Anatase is still the favorite phase for various applications due to its slightly better Fermi level,[2] more stability in the nano form, lower electron−hole pair recombination rates, and better adsorption affinity for organic substances due to better hydroxyl radicals adsorbed and thus better photocatalytic activity.[3] However, the photocatalytic properties of TiO_2 in anatase, rutile, or brookite phases require UV light to activate. To overcome this drawback, doping TiO_2 with other metals might advantageously decrease the band gaps and recombination rate of the excited electron−hole pair and thus increase photoactivity.[4]

The metal and nonmetal doping procedures into TiO_2 could be conducted based on three general approaches including dry mixture, wet impregnation, and molecular mixing.[5] Cu-doped TiO_2 exhibits a low recombination rate and provides numerous trapping centers for charge carriers and enhances photocatalytic performance under sunlight[6] because Cu creates defects in the TiO_2 lattice, which increases the optical absorbance in the visible region, hence improving the photocatalytic activity. The doping leads to new localized energy levels between the conduction and valence bands, inducing band gap narrowing, defects, and oxygen vacancies.[7] Both undoped and doped forms of TiO_2 have been prepared

Received: January 22, 2024
Revised: April 10, 2024
Accepted: April 10, 2024
Published: May 13, 2024

by diverse techniques including sol−gel,[8] hydrothermal,[9] chemical vapor deposition,[10] atomic layer deposition,[11] solvothermal,[12] ion exchange reactions,[13] and coprecipitation.[12] Among these methods, sol−gel—a wet chemical technique—includes simple steps and has the advantages of molecular composition homogeneity, easy controllability, particle size accuracy, reproducibility, and low preparation temperature favorable in the photocatalyst synthesis.[14] TiO_2 prepared by the sol−gel method has been demonstrated to be an effective photoinduced catalyst, which is governed by particle size, phase structure, and light irradiation types.[15]

Electrospun cellulose nanofibers have been extensively studied for varied applications including biomedicine,[16] environment,[17,18] energy storage,[19] drug delivery,[20] air filtration,[21] and water purification.[17] The presence of TiO_2 and copper-doped TiO_2 on CL nanofibers results in self-cleaning effects for the membranes via the photoactive degradation against organic stains under lighting conditions of ultraviolet irradiation and visible light spectrum; moreover, the composite nanofibers can be used for colored water treatment with the recovery ability.[12,22,23] In this study, we investigate the photocatalytic ability of Cu-doped TiO_2 in powder form and after being applied to cellulose nanofiber membranes to decompose methylene blue and organic stains. Samples of TiO_2 doped and nondoped were compared for the optimal doping content and investigating the photoactivity against typically red wine, coffee, and tea colors.

EXPERIMENTAL SECTION

Materials. Titanium isopropoxide—TTIP 97% purity was purchased from Merck, Germany. Copper(II) nitrate hydrate $[Cu(NO_3)_2{\cdot}3H_2O]$ 99.83 wt %, ethanol 99.7%, nitric acid 68%, and methylene blue 99% were acquired from Shanghai Aladdin Biochemical Technology Co., Ltd., China. Cellulose acetate (CA) average Mn ∼ 50,000 was obtained by GPC from Sigma-Aldrich, USA. *N*,*N*-Dimethylformamide (DMF) and acetone (C_3H_6O) were obtained from Macron Fine Chemicals, Germany. The red wine, coffee, and tea were purchased from the local market.

Synthesis. The pristine TiO_2 and Cu-doped TiO_2 were prepared using the sol−gel method. First, TTIP was mixed with ethanol to reach the mol/volume ratio of 0.01 mol/100 mL. The TTIP solution was stirred at 300 rpm at room temperature for 2 h. After that, 0.5 M diluted nitric acid was prepared, whose acidity inhibits the hydrolysis rate of the titanium cation. The nitric acid solution was then added drop by drop to the TTIP solution until reaching the pH of 5 (the pH was determined by using a pH-meter model Mettler FE 20, Switzerland) to form an opaque sol under vigorous stirring and 80 °C for 3 h. The sol then yields turbid gels with white precipitates. For the synthesis of Cu (II)-doped TiO_2 nanoparticles, the copper nitrate was added to the TTIP solution in accordance with the molar ratios of copper nitrate $[Cu(NO_3)_2{\cdot}3H_2O]$:TTIP of 0.5:100, 1:100, 2:100, and 3:100. The pH of copper salt and TTIP solution was also adjusted to 5 and the solution was continuously stirred for 3 h at 80 °C, similar to the TiO_2 synthesis process. Thereafter, the gel was dried for 48 h at 80 °C to form a dry powder. Lastly, the powder was calcined at 450 °C for 3 h with a heating rate of 1 °C/min. The TiO_2 and four samples of Cu-doped TiO_2 were finally received after being finely crushed and denoted as TiO_2, TiO_2−Cu-0.5, TiO_2−Cu-1, TiO_2−Cu-2, and TiO_2−Cu-3, respectively.

Electrospinning and Immobilization of TiO_2 and Cu-Doped TiO_2 onto the Nanofibers. The fabrication of cellulose nanofiber membranes was performed by the electrospinning method. The preparation of electrospinning solution was conducted by dissolving 1.0 g of CA in a mixture of 2.25 g of DMF and 3.4 g of acetone and stirred for 12 h at room temperature to ensure complete dissolution. The electrospinning solution was loaded into a 10 mL syringe with a metallic needle (the inner diameter was 0.4 mm), and the injection rate of the electrospinning solution was 0.45 mL/h. A voltage supply (Gamma High Voltage Research Inc.) was connected to the needle tip using an alligator clip. The voltage of 16 kV was applied between the needle tip and a flat collector (stainless steel wire mesh covered with aluminum foil, 30 cm × 30 cm), and the distance was set to 20 cm. The electrospinning was carried out at room temperature. After electrospinning, the obtained CA mats were peeled off the collector. The deacetylation process using 0.05 M NaOH was performed to remove the acetate radicals. After 24 h of immersing CA mats in alkaline solution, the CL nanofibers were removed and washed in the deionized water until the pH became neutral and dried at 80 °C for 24 h.

The immobilization of the metal oxide nanoparticles on the CL nanofibers was performed by a dip-coating technique. The amount for each sample of TiO_2, TiO_2−Cu-0.5, TiO_2−Cu-1, TiO_2−Cu-2, and TiO_2−Cu-3 nanoparticles was calculated to be 10 wt % of CL nanofibers and then dispersed in ethanol (1 mg/mL) in glass beakers. The beakers containing CL nanofiber membranes were ultrasonicated by utilizing an ultrasonic cleaner (DC-250H, MRC) at 30 kHz at room temperature for 30 min. The composite CL webs were eventually taken out and dried at room temperature, namely, CL, CL-TiO_2, CL-TiO_2−Cu-0.5, CL-TiO_2−Cu-1, CL-TiO_2−Cu-2, and CL-TiO_2−Cu-3.

Photocatalytic Activity. The photocatalytic degradation of reactive methylene blue using TiO_2 and Cu-doped TiO_2 was investigated under a 300 W xenon lamp with a 420 nm UV-cutoff filter (420−780 nm) (LOT, Germany) as a visible light source and the UV radiation source emitted from a 60 W fluorescent lamp, with a wavelength of 254 nm (US Sterilizer lamp). The xenon lamp and UV lamp were placed 15 cm away from the MB solution containing semiconductor nanoparticles during the irradiation. The samples were irradiated over 90 min with a xenon lamp and 180 min with a UV lamp. The tested degradation specimens were measured each 15 min time interval. The decomposition experiments were carried out using an initial concentration of 10 ppm; 10 mL of methylene blue solution containing 1 mg of doped or undoped TiO_2 nanoparticles was stirred at 500 rpm for 15 min without light irradiation to check the initial adsorption. Five mL of each solution was then pipetted out and centrifuged at 9000 rpm to collect clear solution without the solid part. The solution specimens were then transferred into a UV quartz cuvette with a volume of 3.5 mL (Sigma-Aldrich) for photocatalytic measurement. The MB concentration was determined by an Avantes UV−vis spectrometer at an absorptive peak of 664 nm wavelength.

Characterization Methods. The crystalline phase and particle size of pure and Cu-doped TiO_2 nanoparticles were analyzed by X-ray diffraction (XRD, Bruker D8-ADVANCE diffractometer, Germany) equipped with Cu Kα (k = 0.154 Å) radiation, operating at 40 kV with 30 mA. The diffraction data were recorded for 2 h in the range of 2θ from 20 to 80° with a

https://doi.org/10.1021/acsomega.4c00656
ACS Omega 2024, 9, 22734−22743

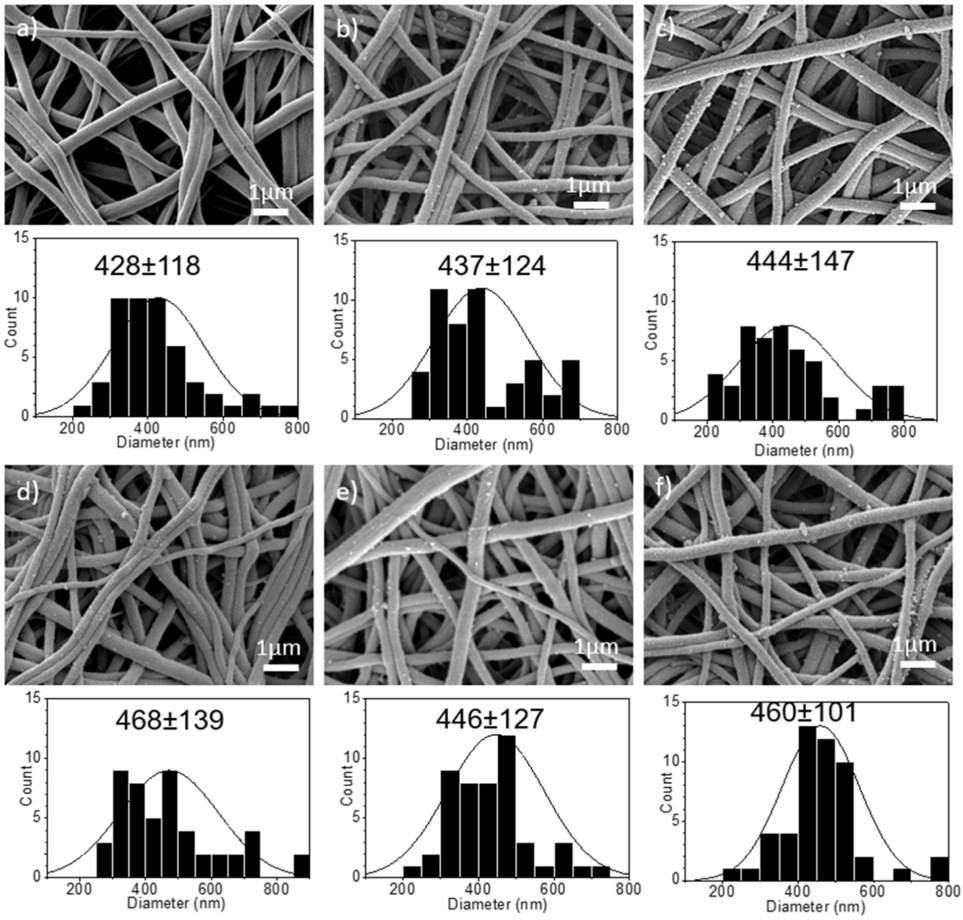

Figure 1. FE-SEM images of (a) CL membranes and CL membranes coated with (b) TiO_2, (c) TiO_2−Cu-0.5, (d) TiO_2−Cu-1, (e) TiO_2−Cu-2, and (f) TiO_2−Cu-3.

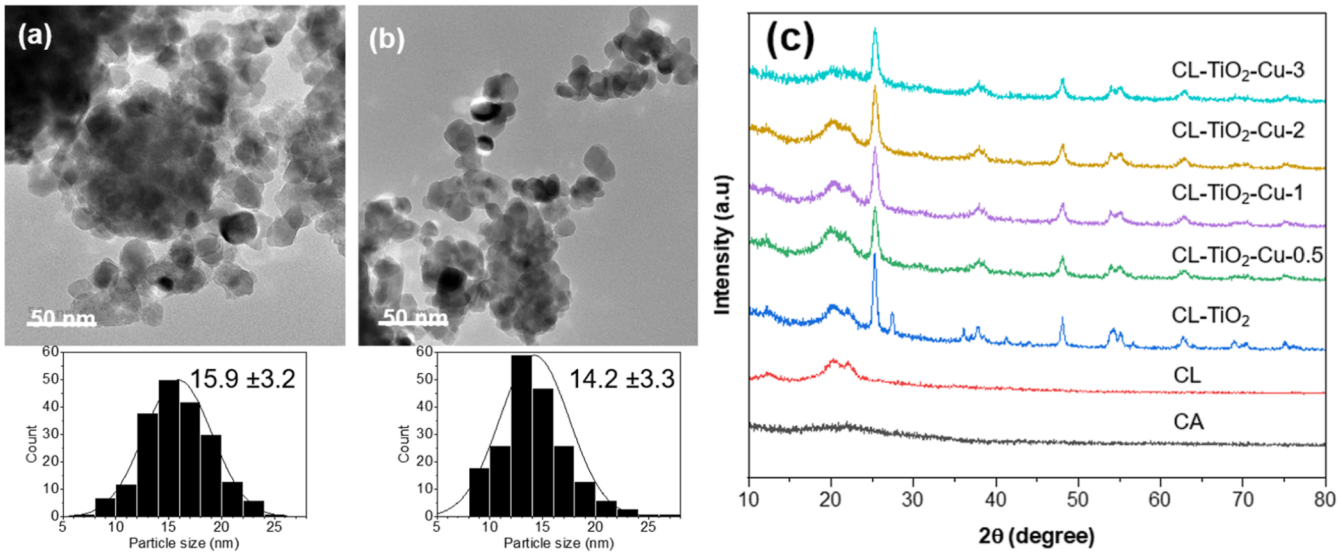

Figure 2. TEM images and particle size distribution of (a) TiO_2 and (b) TiO_2-doped Cu 3% and XRD pattern of the CA, CL, and CL with nanoparticles.

scanning rate of 5°/min. The characterization of the composite cellulosic membrane chemistry was carried out by Fourier transform infrared (FTIR) spectroscopy (Thermo Scientific Nicolet 6700 spectrometer) using a resolution of 2 cm^{-1} in the range of 4000−400 cm^{-1}. The surface morphologies and structures of materials were investigated by field emission scanning electron microscopy (FE-SEM, Hitachi S-4800, JAPAN) and transmission electron microscopy (TEM, JEM 1010—JEOL with a voltage of 100 kV, JAPAN). The composition of the samples was observed with energy-dispersive X-ray spectroscopy (EDS, SU-8000 microscope, Hitachi, Japan). UV−vis diffuse reflectance spectroscopy

https://doi.org/10.1021/acsomega.4c00656
ACS Omega 2024, 9, 22734−22743

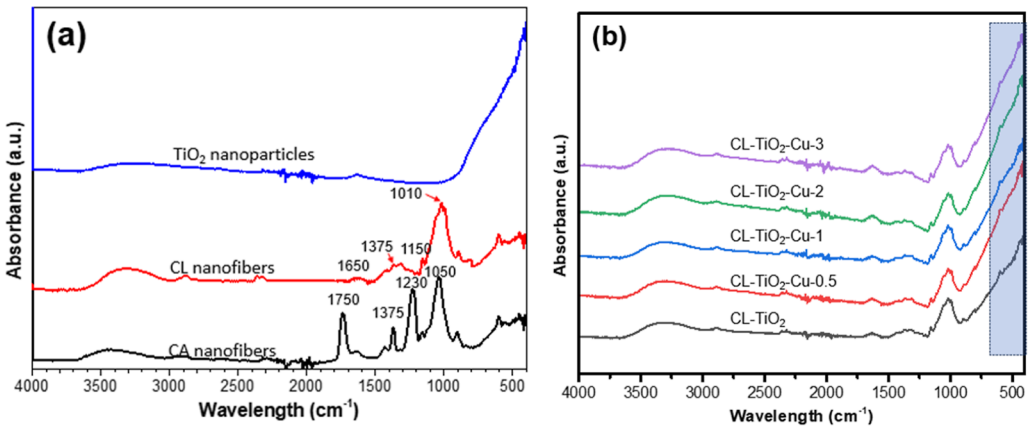

Figure 3. FTIR spectra of (a) CA, CL, and TiO_2 and (b) CL-TiO_2 and other CL nanofibers containing Cu-doped TiO_2 nanoparticles.

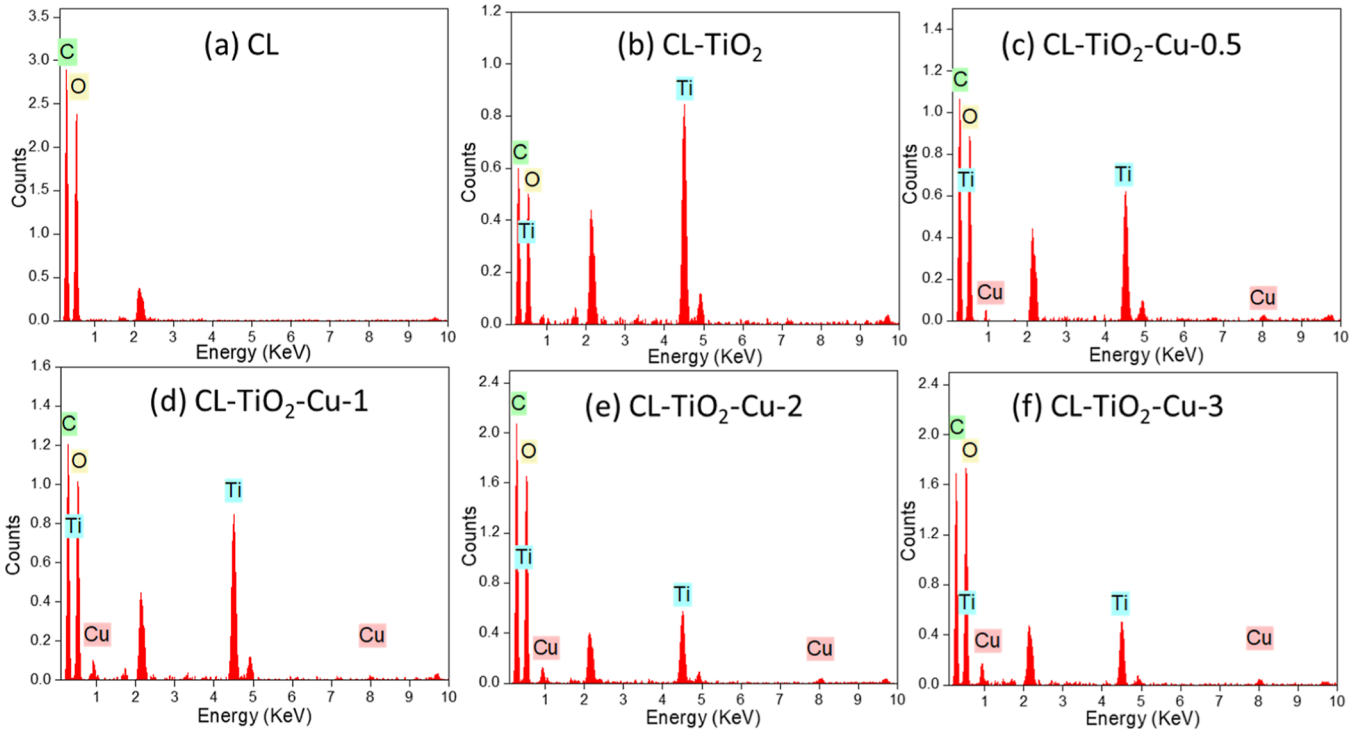

Figure 4. EDS spectra of (a) CL, (b) CL-TiO_2, (c) CL-TiO_2−Cu-0.5, (d) CL-TiO_2−Cu-1, (e) CL-TiO_2−Cu-2, and (f) CL-TiO_2−Cu-3.

(DRS) spectra were collected by the Shimadzu UV-2600 UV−vis spectrophotometer. The tensile strength, elongation at break, and Young's modulus were recorded by the tensile test five times for each sample (Tenso Lab 2512A, Mesdan tensile testing machine).

RESULTS AND DISCUSSION

Morphological and Structural Analysis. Morphological images of CL, CL-TiO_2, CL-TiO_2−Cu-0.5, CL-TiO_2−Cu-1, CL-TiO_2−Cu-2, and CL-TiO_2−Cu-3 were captured, showing bead-free nanofibers with average diameters of 428 ± 118, 437 ± 124, 444 ± 147, 468 ± 139, 446 ± 127, and 460 ± 101 nm in Figure 1. The CL and CL-containing nanoparticles have similar morphologies and size distributions ranging from 200 to 800 nm. The CL nanofibers present a smooth surface, and after the incorporation of TiO_2 or TiO_2-doped Cu, the nanofibers present white small dots on the surfaces and the diameter increases of the nanofibers were attributed to the attachment of nanoparticles on the surface. For CL-TiO_2- and CL-TiO_2-doped samples, the nanoparticles dispersed homogeneously on the CL scaffold, resulting in relatively coarse and rough morphologies for the composite nanofibers.

The morphological and structural characteristics of pristine and Cu-doped TiO_2 NPs were further investigated by using TEM. Figure 2 shows that the average particle sizes of TiO_2 and TiO_2−Cu-3 were 15.9 ± 3.2 and 14.2 ± 3.3 nm, respectively. The particle shape was spherical, and obviously, when doped with 3% Cu, the size decreased. TEM images present large aggregates with a size larger than 100 nm consisting of smaller nanoparticles.

The XRD patterns of CA, CL, and CL with nanoparticles are shown in Figure 2c. The diffraction peaks were indexed to (101), (004), (200), (105), (211), and (204) planes at 2θ = 25.5, 38.0, 48.0, 54.0, 55.0, and 63.0, respectively, confirming the synthesizing success of the TiO_2 anatase phase (JCPDS no. 21-1272). Furthermore, there is an intense diffraction peak

https://doi.org/10.1021/acsomega.4c00656
ACS Omega 2024, 9, 22734−22743

noticed for rutile phase at 2θ = 27.5 corresponding to the (110) plane (JCPDS no. 21-1276). Peaks are absent for Cu, indicating that Cu was doped into the TiO_2 lattice, but the amount is not enough to form crystalline regions. The average crystallite size of the samples was calculated from fwhm (full width at half-maximum) following the formula $D = k\lambda/(\beta \cos \theta)$, where D represents the average crystallite size, λ represents the wavelength of incident X-ray, β represents the fwhm of the peak, and θ represents the scattering angle. With the increase of the Cu concentration, the average crystallite size decreases from 16.28 ± 5.26 to 14.74 ± 6.41 nm according to TEM results. Doping was assumed to be the reason for smaller sizes of doped TiO_2 compared to that of undoped nanoparticles.

Fourier Transform Infrared Analysis. Figure 3a presents the FT-IR spectra of the CA and CL nanofibers. The CA spectrum shows signature peaks at 1750, 1375, 1230, and 1050 cm^{-1} corresponding to C═O vibration, C−CH_3 vibration, C−O−C stretching vibration, and C−O stretching.[24] The peak at 1750 cm^{-1} is the stretching vibration of the acetyl group and the peak at 1230 cm^{-1} corresponds to the vibration of C−O−C, both are characteristic peaks of CA nanofibers. After the deacetylation process, the CL nanofibers present the enhanced band from 3100 to 3500 cm^{-1} and the peak at 1650 cm^{-1} is ascribed to the −O−H stretching and the bending vibration of absorbed H_2O.[8] For the spectrum of TiO_2 nanoparticles, in the region from 3000 to 3600 cm^{-1}, the peaks at 1635 cm^{-1} and around 400 cm^{-1} are distributed to the stretching of the −OH group, Ti−OH, and Ti−O. The doping of Cu into the TiO_2 lattice does not exhibit any signals or peaks observed from the spectra, and the amount of Cu-doped into the TiO_2 matrix could not be recognized using the FTIR method.

Energy-Dispersive X-ray Spectroscopy. The EDS shows the chemical composition of various composite nanofibers, Figure 4. The presence of Ti in the composite CL nanofibers compared with pristine CL nanofibers confirms that TiO_2 and Cu-doped TiO_2 nanoparticles were successfully attached onto the surfaces of CL nanofibers.

The elemental analyses of TiO_2 and Cu-doped TiO_2 nanoparticles are illustrated in Figure 4b−f. The intense peaks in pure TiO_2 are associated with the average atomic mass percentage of O (52.85%) and Ti (11.70%) elements. The measured Cu weight factors are around 0.60, 0.14, 0.84, 0.95, and 1.10% for 0.5, 1, 2, and 3% doping, showing that the presence of dopant is increased corresponding to the larger loading amount of Cu.

Tensile Strength. The tensile stress−strain of CA, CL, and CL-containing photocatalytic nanoparticles is shown in Figure 5 and Table 1. The tensile strength of the nanofibrous mats is highly needed for practical uses, and in general, cellulose nanofibers possess good mechanical characteristics. The CL nanofibers after the deacetylation process present much better stress at break compared to CA nanofibers due to the increased hydrogen bonding between fibers. A tensile strength of 3.0 MPa was only obtained for CA nanofibers, but the markedly larger value of 9.7 MPa for CL demonstrated the role of newly formed −OH groups on the fiber surfaces. Internanofiber hydrogen bonding interaction was reduced in the cases of TiO_2 and Cu-doped TiO_2 particles integrated into the CL mats, resulting in the significant reductions of strength with values from 7.53 ± 0.59 MPa to 6.88 ± 0.16 MPa. The amount of decrease in the cellulose nanofiber membrane's tensile strength implies that the immobilization treatment changes the physical properties of the membrane.

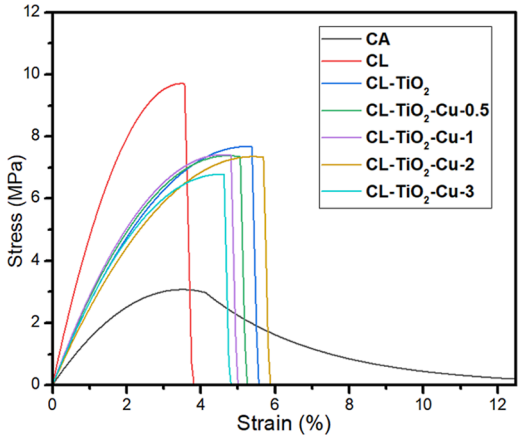

Figure 5. Tensile strength of CA, CL, and composite CL nanofibers.

Table 1. Tensile Strength, Elongation at Break, and Young's Modulus of Composite CL Nanofibers

sample	tensile strength (MPa)	elongation at break (%)	Young's modulus (MPa)
CA	3.06 ± 0.47	16.76 ± 5.54	140.63 ± 4.42
CL	9.72 ± 0.31	3.30 ± 0.34	412.62 ± 14.51
CL-TiO_2	7.53 ± 0.59	5.30 ± 0.20	120.31 ± 4.42
CL-TiO_2−Cu-0.5	7.33 ± 0.27	4.74 ± 0.32	239.81 ± 5.84
CL-TiO_2−Cu-1	7.48 ± 0.33	4.66 ± 0.37	245.43 ± 6.19
CL-TiO_2−Cu-2	7.40 ± 0.40	5.49 ± 0.31	216.31 ± 4.42
CL-TiO_2−Cu-3	6.88 ± 0.16	4.66 ± 0.38	226.81 ± 5.84

UV−Vis DRS Analysis. The UV−vis absorbance spectra of TiO_2 nanoparticles with different Cu-doping contents and undoped TiO_2 were recorded in DI water and are illustrated in Figure 6, which are the plots of $(\alpha h\nu)^2$ versus photon energy ($h\nu$) of TiO_2. The energy band gap was obtained by extrapolating the plot and drawing a linear relation. Compared with the absorbance spectrum of undoped TiO_2 nanoparticles, Cu-doped TiO_2 nanoparticles have a higher light harvest performance reflected by not only the widening of its UV absorbance peak but also the evident enhancement of light absorbance covering the whole visible range. The redshift of the band gap can be obtained by the plot of $(Ah\nu)^2$ and $h\nu$ (E_g) (A is the absorbance; h is the Planck constant; and ν is the frequency of incident light), which reveals that the band gap shifts from 3.09 eV for undoped TiO_2 to 2.98 eV for Cu-doped 3% TiO_2. Therefore, doping is important to enhance catalytic activity and for practical applications. The mechanisms could be detailed as electrons and holes generated by the photon absorption migrate to the surface of photocatalytic nanoparticles to activate redox reactions; however, the charge carrier recombination hinders the whole process. Modification with copper, therefore, can affect the particle sizes and surface structures of TiO_2 photocatalysts. More importantly, metal ion doping can make new valence bands above the original ones, thus developing visible light-harvesting photocatalysts.[25]

Photocatalytic of Doped and Undoped TiO_2 Powder under UV Light and Xenon Light. The photocatalytic activity of TiO_2 and Cu-doped TiO_2 nanoparticles was determined utilizing photocatalytic reactions in an aqueous dye solution of methylene blue (the amount of MB is 10 ppm for experiments) under both ultraviolet light (60 W) and xenon light (300 W), thus demonstrating the effectiveness of doping contents of Cu. After mixing the catalyst in the MB

https://doi.org/10.1021/acsomega.4c00656
ACS Omega 2024, 9, 22734−22743

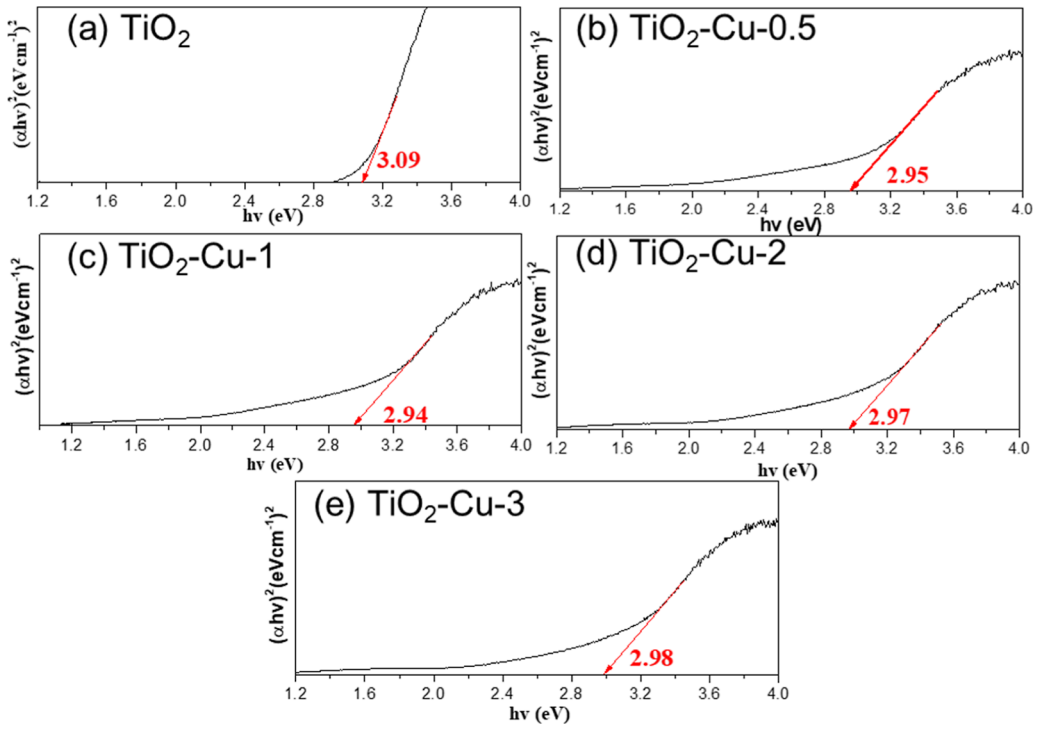

Figure 6. UV−vis absorption spectra of TiO_2 and Cu-doped TiO_2 nanoparticles with different Cu contents: (a) TiO_2, (b) TiO_2−Cu-0.5, (c) TiO_2−Cu-1, (d) TiO_2−Cu-2, and (e) TiO_2−Cu-3.

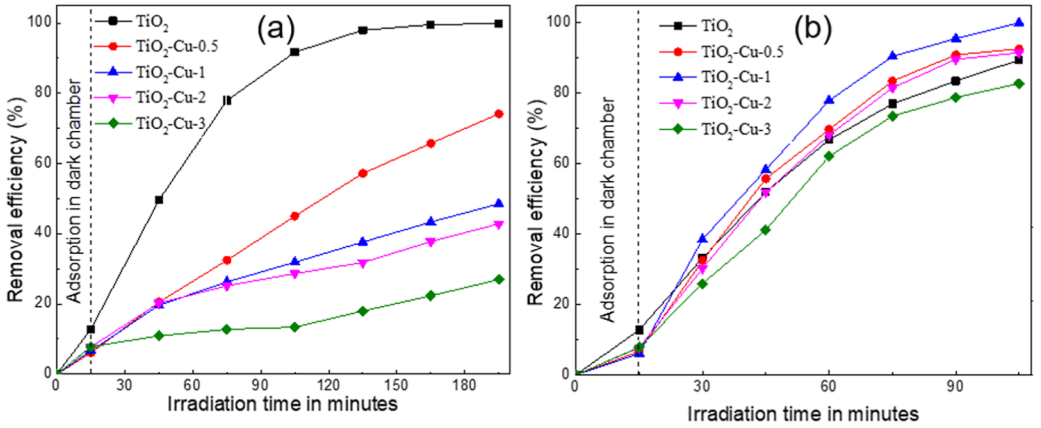

Figure 7. MB photocatalytic degradation efficiency of TiO_2 and doped TiO_2 samples under (a) UV radiation and (b) xenon radiation.

solution for 15 min in the dark, the photocatalytic degradation of the samples was carried out under UV light and xenon light. The photocatalytic efficiency of Cu-doped TiO_2 was compared with that of pure TiO_2 as a function of time for various periods and are displayed in Figure 7. The experiments without photocatalysts show that the concentration of MB had no decrease over time.

A crucial factor in determining the rate of photocatalytic degradation is adsorption. In the dark, the MB molecules are adsorbed onto photocatalyst's surfaces, and with light irradiation, electron donors transfer electrons from the valence band to the conduction band of the catalyst.[26] Figure 7a,b shows that pure titanium dioxide nanoparticles have the ability to adsorb more MB molecules than copper-doped titanium dioxide nanoparticles.

TiO_2 nanoparticles are more efficient in terms of MB removal than Cu-doped TiO_2 nanoparticles in terms of UV light illumination. The percentage of dye degradation for the TiO_2 sample in the presence of UV light was observed at 99.89% after 3 h of irradiation. Increasing the Cu loading in TiO_2 (0.5, 1, 2, and 3%) decreased methylene blue degradation percentages under UV light influence to 74, 49, 43, and 27%, respectively. The degradation rates of the MB dye for doped catalysts were slower compared to that for the undoped one. After being doped, under UV irradiation, a negative trend is presumed to overwhelm. Cu ions are negatively charged by the electrons and converted into recombination for positive holes, which causes a decline in the amount of hydroxyl radicals; moreover, the Cu ions cover the surface of TiO_2, thereby decreasing the photocatalytic activity.[27]

In contrast, when exposed to xenon light, the photocatalytic degradation efficiency was enhanced due to the loading of Cu in TiO_2, Figure 5b. Among all doped TiO_2 nanoparticles, the TiO_2−Cu-1 sample has the highest activity in eliminating MB. When using a xenon light source, 99% of MB was removed from the solution in the presence of the doping sample within

https://doi.org/10.1021/acsomega.4c00656
ACS Omega 2024, 9, 22734−22743

105 min of reaction, whereas the performance of TiO_2 nanoparticles is 89.4%. However, when the content of Cu doping increases to 2%, the photocatalytic performance decreases to a level of 91.5% and tends to maintain the trend when increasing the Cu-doped ratio to 3%. In general, doping with Cu narrows the band gap and thus helps Cu-doped TiO_2 absorb xenon light better during the dye degradation process. Nevertheless, a higher amount of Cu dopants incorporating the TiO_2 lattice might trap photogenerated electrons excessively and thus limit photoinduced activity.[28] Besides, a high concentration of Cu in TiO_2 may lower the TiO_2-specific surface area and reduce the quantity of active sites available for adsorption and reaction with methylene blue molecules, resulting in a decrease in degradation efficiency. It is noteworthy that the photocatalytic degradation of MB dye was better and faster under xenon light compared to UV light for doped nanoparticles, which was caused by the high energy of xenon light.[29]

Figure 8 is the proposed mechanism of TiO_2 and Cu-doped TiO_2 nanoparticles coated on cellulose nanofiber membranes

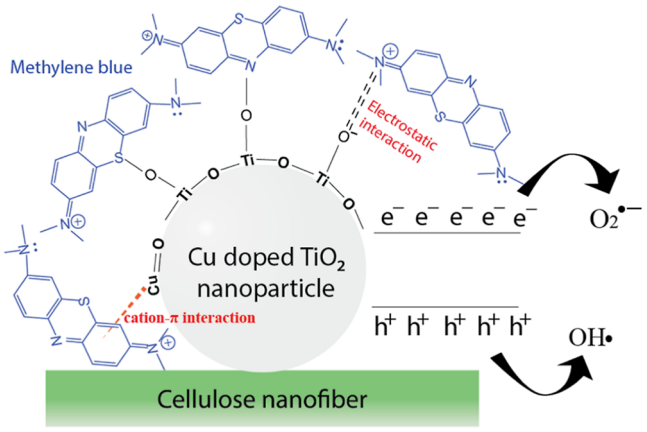

Figure 8. Proposed mechanisms of MB adsorption and degradation by cellulose nanofibers coated with TiO_2 and Cu-doped TiO_2 nanoparticles.

for the adsorption and degradation process. The nanoscale of particles increases the high surface area, which enhances the physical adsorption of methylene blue on TiO_2 and Cu-doped TiO_2 nanoparticles. The presence of functional groups promotes the adsorption of dye molecules through chemical interaction. It is suggested that the adsorption of methylene blue on the catalyst involves two different potential interactions. The first adsorption site of TiO_2 for MB was the interaction between NH^{2+} on MB as a cationic form of adsorbate molecule and O^{2-} on TiO_2 samples, and the chemical bond is the electrostatic interaction. The second one is through the hydrogen bonding appearing between the amine groups on methylene blue with Ti−OH. Similar mechanisms on the interaction of TiO_2 and MB have been proposed in several studies.[30] After doping with Cu ions in the titanium oxide structure, photocatalysts enhance the adsorptive capacity by forming cation−π interactions with the dye's aromatic rings.[31]

Under light irradiation, TiO_2 was photoexcited to generate an electron−hole pair on the surface of the catalyst. The direct oxidation of adsorbed water by the hole in the valence band of the catalyst produces the hydroxyl radical $OH^{\bullet}$ and electron in the conduction band of the catalyst can reduce the molecular oxygen to superoxide anion. The hydroxyl radical was the main responsible species for the degradation of methylene blue molecules. With the doping, an enhanced photocatalytic process could also be explained by the increased generation of highly oxidizing hydroxyl radicals ($OH^{\bullet}$)[32] via the Photon−Fenton reaction of Cu ions in the presence of a superoxide anion.

Photodegradation Performance for Some Organic Stains on Fabrics, Typically Red Wine, Coffee, and Tea. With the intention of demonstrating the photocatalytic self-cleaning ability of the Cu-doped TiO_2-coated CL nanofiber membrane, some organic stains, particularly red wine, coffee, and tea, were applied to the surface of the nanofibers. To investigate the stain degradation, the functionalized samples (5 cm × 5 cm) were dipped in a solution of each organic stain for 5 s for staining and then dried at room temperature. These samples were continuously exposed to xenon light at a distance of 19 cm from the light source. An aqueous solution of coffee and tea stains was prepared by mixing 1.0 g of coffee or tea in 50 mL of deionized water. Then coffee, tea, and red wine stains were introduced on the composite CL nanofibers in an amount of 10 wt %. According to the results from MB photocatalytic degradation efficiency, 1% Cu-doped TiO_2 gave the highest performance among all doped nanoparticles under visible light illumination. Therefore, in this experiment, we used the CL-TiO_2−Cu-1 membrane to demonstrate the self-cleaning activity.

The K/S value represents the color depth of the nanofibers and can be used as decoloration indicators. The K/S values as a function of time were measured with the help of a Ci4200 SpectroPhotometer with the D 65 illuminant and 100 standard observer from 400 to 700 nm with 10 nm intervals. The K/S values for all samples were calculated according to the Kubelka−Munk equation. The decrease in K/S values indicates that the stains are fading. $K/S = (1 - R)^2/2R$, where K is the absorption coefficient, S is the scattering coefficient, and R is the reflectance of the coated nanocellulose membranes. The K/S values were measured every 2 h exposed to xenon light. The CL-TiO_2−Cu-1 samples with organic stains were exposed to a light source for 24 h.

Figure 9a shows the average K/S values of stained samples measured at different times; the K/S values present similar trend, reducing as the illumination time increases. Based on the results, organic stains including coffee, tea, and red wine were practically removed from the CL-TiO_2−Cu-1 membranes. The decoloration process showed great results that % degradation values of coffee, red wine, and tea colors on the membrane were 83.1, 86.0, and 74.6%, respectively, after 24 h of irradiation.

Besides, the efficiency of the self-cleaning membrane could be identified based on the color difference between the treated samples and the control samples, measured via the CIE $L^*a^*b^*$. L^* is lightness from black (0) to white (+100), a^* signifies the red/green value ($+a^*$ was the red axis, $-a^*$ was the green axis), and b^* signifies the yellow/blue value ($+b^*$ was the yellow axis, $-b^*$ was the blue axis). dE^* represents the total color difference and is calculated using the following formula: $dE^* = (dL^{*2} + da^{*2} + db^{*2})^{1/2}$.

The photocatalytic activity of the nanocellulose membrane after staining with coffee, red wine, and tea and exposure to visible light is shown in Table 2. To evaluate the self-cleaning capabilities of photocatalytic coating, color measurements were

https://doi.org/10.1021/acsomega.4c00656
ACS Omega 2024, 9, 22734−22743

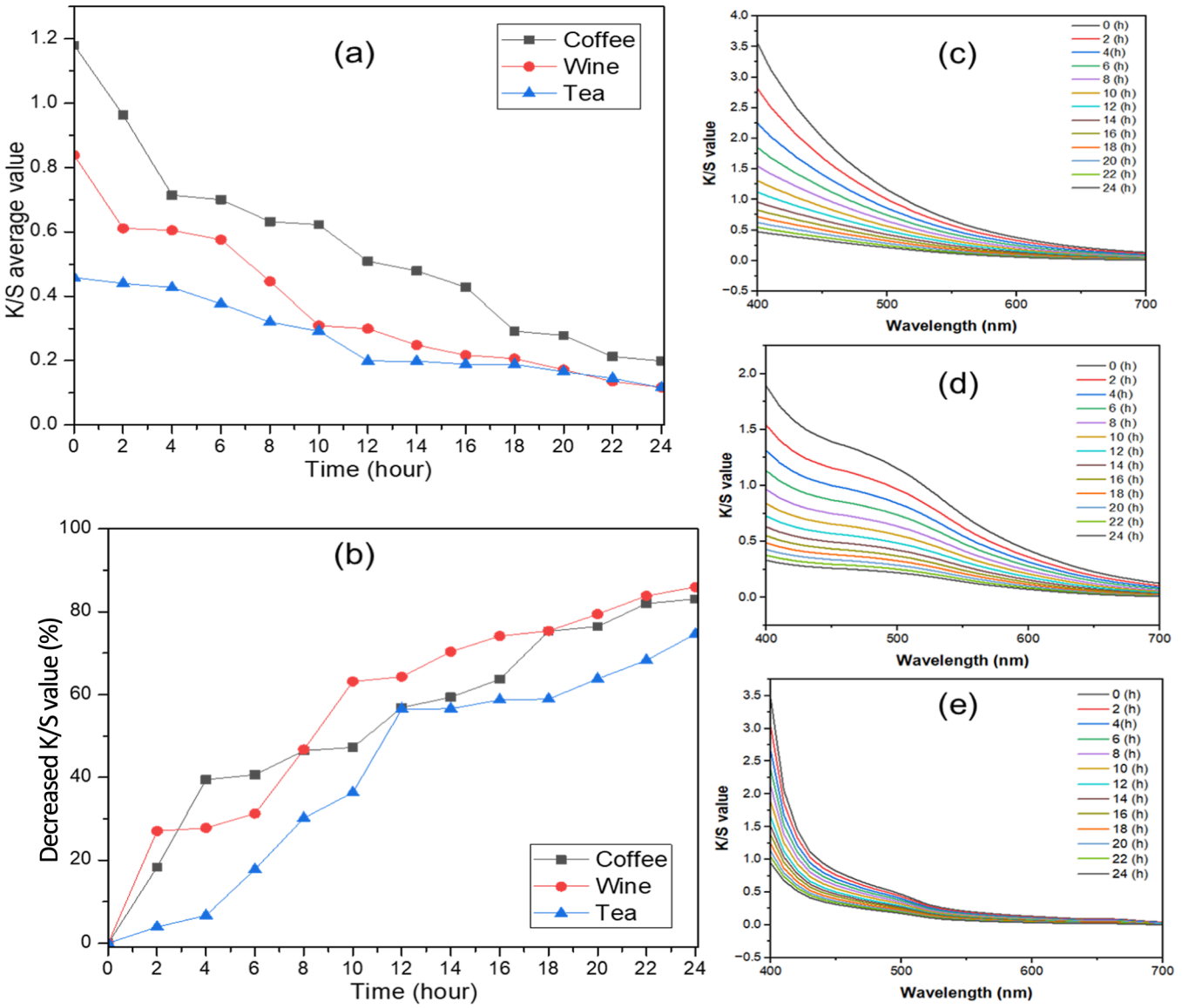

Figure 9. (a) *K*/*S* average values. (b) Percentage decrease of *K*/*S* average values and evolution of *K*/*S* values as a function of time during xenon light irradiation of samples stained with (c) coffee, (d) red wine, and (e) tea.

Table 2. Color Difference (d*E) of CL-TiO_2−Cu-1 Stained with Coffee, Red Wine, and Tea under Xenon Irradiation**

sample	d*E**		
	coffee	red wine	tea
CL-TiO_2−Cu 0.5	0.00	0.00	0.00
0 h	19.41	24.64	34.45
2 h	16.86	24.24	29.93
4 h	13.26	23.58	29.70
6 h	13.17	22.57	28.89
8 h	11.44	20.95	25.65
10 h	10.66	20.05	21.15
12 h	9.07	15.42	20.49
14 h	8.08	15.41	18.39
16 h	7.04	15.08	16.99
18 h	6.82	14.80	16.55
20 h	5.40	13.72	14.55
22 h	5.36	12.47	12.10
24 h	4.38	10.28	10.88

made for different periods of time (from 0 to 24 h) of the experiment using the membrane without stain as references.

As can be seen in Table 2, from the value of the total color difference (d*E**), organic compounds on the CL membranes after 24 h of light exposure are effectively degraded. With the coffee stain, d*E** decreased from 19.41 at 0 h to 4.38 at 24 h, showing 77.43% self-cleaning efficiency, while with the red wine, d*E** decreased from 24.64 at 0 h to 10.28 at 24 h, illustrating 58.30% self-cleaning efficiency. For the tea, d*E** decreased from 34.45 at 0 h to 10.88 at 24 h, demonstrating 68.42% self-cleaning efficacy. The decreases in d*E** indicate that color organic compounds were removed from the membranes, and thus, Cu-doped TiO_2 nanoparticle-treated CL membranes have self-cleaning abilities. Photocatalysis by Cu-doped TiO_2 after immobilization to the nanofibrous surface is considered an effective method for self-cleaning application of membranes against various organic staining agents and particularly renders the membranes to be visible light responsive.[33] In general, the self-cleaning performance reaches more than 50%. Figure 10 shows the changes in color

https://doi.org/10.1021/acsomega.4c00656
ACS Omega 2024, 9, 22734−22743

Figure 10. Color changes of CL-TiO_2−Cu-1-containing stains from coffee, tea, and red wine during the period of time from 0 to 22 h under xenon light irradiation.

of the CL membranes coated with Cu-doped TiO_2 with red wine, coffee, and tea stains. The organic strains were significantly discolored after 22 h of light irradiation.

CONCLUSIONS

In conclusion, using the electrospinning technique, we successfully synthesized CL nanofibers with average diameters below 500 nm. Doping TiO_2 with Cu led to high photodegradation performance. The Cu-doped TiO_2 molar ratio in the nanocomposite was found to have a pronounced effect on dye removal and self-cleaning effects. In the experiment, Cu-doped TiO_2 nanoparticles can increase the photodegradation of the MB dye under xenon light irradiation. The photodegradation effectiveness is nearly 99% after 105 min for TiO_2−Cu-1, proving the dye removal effectiveness. Our research has shown that the sol−gel synthesis of Cu-doped TiO_2 is a highly effective and economical approach to pollutant adsorption. In this study, the semiconductor nanoparticles were successfully immobilized onto the CL nanofiber membranes by a dip-coating method. These membranes exhibit the ability to self-clean with organic compounds such as coffee, green tea, and red wine, with a removal of more than 50% after 24 h under xenon illumination. These findings imply that CL membrane-coated Cu-doped TiO_2 may be an advantageous element in filters, protective clothing, and environmental solutions.

AUTHOR INFORMATION

Corresponding Authors

Duy-Nam Phan − *School of Materials Science and Engineering, Hanoi University of Science and Technology, Hanoi 100000, Vietnam*; Email: nam.phanduy@hust.edu.vn

Ick-Soo Kim − *Nano Fusion Technology Research Group, Institute for Fiber Engineering (IFES), Interdisciplinary Cluster for Cutting Edge Research (ICCER), Shinshu University, Ueda 386-8567, Japan*; orcid.org/0000-0003-2126-0381; Email: kim@shinshu-u.ac.jp

Authors

Thi Ngat Tran − *School of Materials Science and Engineering, Hanoi University of Science and Technology, Hanoi 100000, Vietnam*

Phuong-Linh Nguyen − *School of Materials Science and Engineering, Hanoi University of Science and Technology, Hanoi 100000, Vietnam; Hanoi Industrial Textile Garment University, Hanoi 100000, Vietnam*

Minh Thang Le − *School of Chemistry and Life Science, Hanoi University of Science and Technology, Hanoi 100000, Vietnam*; orcid.org/0000-0001-6094-0123

Azeem Ullah − *Nano Fusion Technology Research Group, Institute for Fiber Engineering (IFES), Interdisciplinary Cluster for Cutting Edge Research (ICCER), Shinshu University, Ueda 386-8567, Japan*

Complete contact information is available at: https://pubs.acs.org/10.1021/acsomega.4c00656

Funding

This work was funded by the Vietnam Ministry of Education and Training under grant no. B2022-BKA-18.

Notes

The authors declare no competing financial interest.

REFERENCES

(1) Rathore, N.; Kulshreshtha, A.; Shukla, R. K.; Sharma, D. Optical, structural and morphological properties of Fe substituted rutile phase TiO_2 nanoparticles. *Phys. B* **2021**, *600*, 412609.

(2) Zhou, Z.; Gao, J.; Zhang, G.; Dong, Y.; Wang, Z.; Li, J.; Lyu, J. Optimizing graphene-TiO_2 interface properties via Fermi level modulation for photocatalytic degradation of volatile organic compounds. *Ceram. Int.* **2020**, *46* (5), 5887−5893.

(3) Li, G.; Fang, K.; Ou, Y.; Yuan, W.; Yang, H.; Zhang, Z.; Wang, Y. Surface study of the reconstructed anatase TiO_2 (001) surface. *Prog. Nat. Sci.: Mater. Int.* **2021**, *31* (1), 1−13.

(4) Katal, R.; Masudy-Panah, S.; Tanhaei, M.; Farahani, M. H. D. A.; Jiangyong, H. A review on the synthesis of the various types of anatase TiO_2 facets and their applications for photocatalysis. *Chem. Eng. J.* **2020**, *384*, 123384.

(5) Phan, D.-N.; Rebia, R. A.; Saito, Y.; Kharaghani, D.; Khatri, M.; Tanaka, T.; Lee, H.; Kim, I.-S. Zinc oxide nanoparticles attached to polyacrylonitrile nanofibers with hinokitiol as gluing agent for synergistic antibacterial activities and effective dye removal. *J. Ind. Eng. Chem.* **2020**, *85*, 258−268.

(6) Phan, D.-N.; Dorjjugder, N.; Saito, Y.; Khan, M. Q.; Ullah, A.; Bie, X.; Taguchi, G.; Kim, I.-S. Antibacterial mechanisms of various copper species incorporated in polymeric nanofibers against bacteria. *Mater. Today Commun.* **2020**, *25*, 101377.

(7) Gupta, T.; Samriti; Cho, J.; Prakash, J. Hydrothermal synthesis of TiO_2 nanorods: formation chemistry, growth mechanism, and tailoring of surface properties for photocatalytic activities. *Mater. Today Chem.* **2021**, *20*, 100428.

(8) Phan, D.-N.; Dorjjugder, N.; Khan, M. Q.; Saito, Y.; Taguchi, G.; Lee, H.; Mukai, Y.; Kim, I.-S. Synthesis and attachment of silver and copper nanoparticles on cellulose nanofibers and comparative antibacterial study. *Cellulose* **2019**, *26*, 6629−6640.

(9) Phan, D.-N.; Dorjjugder, N.; Saito, Y.; Taguchi, G.; Ullah, A.; Kharaghani, D.; Kim, I.-S. The synthesis of silver-nanoparticle-anchored electrospun polyacrylonitrile nanofibers and a comparison with as-spun silver/polyacrylonitrile nanocomposite membranes upon antibacterial activity. *Polym. Bull.* **2020**, *77*, 4197−4212.

(10) Alotaibi, A. M.; Sathasivam, S.; Williamson, B. A.; Kafizas, A.; Sotelo-Vazquez, C.; Taylor, A.; Scanlon, D. O.; Parkin, I. P. Chemical vapor deposition of photocatalytically active pure brookite TiO_2 thin films. *Chem. Mater.* **2018**, *30* (4), 1353−1361.

(11) Mali, S. S.; Shim, C. S.; Park, H. K.; Heo, J.; Patil, P. S.; Hong, C. K. Ultrathin atomic layer deposited TiO_2 for surface passivation of hydrothermally grown 1D TiO_2 nanorod arrays for efficient solid-state perovskite solar cells. *Chem. Mater.* **2015**, *27* (5), 1541−1551.

(12) Jatoi, A. W.; Kim, I. S.; Ni, Q.-Q. Cellulose acetate nanofibers embedded with AgNPs anchored TiO_2 nanoparticles for long term excellent antibacterial applications. *Carbohydr. Polym.* **2019**, *207*, 640−649.

(13) Yang, Q.; Hu, M.; Guo, J.; Ge, Z.; Feng, J. Synthesis and enhanced photocatalytic performance of Ag/AgCl/TiO_2 nano-

https://doi.org/10.1021/acsomega.4c00656
ACS Omega 2024, 9, 22734−22743

composites prepared by ion exchange method. *J. Mater.* **2018**, *4* (4), 402−411.
(14) (a) Pant, B.; Park, M.; Park, S.-J. Recent advances in TiO_2 films prepared by sol-gel methods for photocatalytic degradation of organic pollutants and antibacterial activities. *Coatings* **2019**, *9* (10), 613. (b) Simon, S. M.; George, G.; Sajna, M.; Prakashan, V.; Jose, T. A.; Vasudevan, P.; Saritha, A.; Biju, P.; Joseph, C.; Unnikrishnan, N. Recent advancements in multifunctional applications of sol-gel derived polymer incorporated TiO_2-ZrO_2 composite coatings: a comprehensive review. *Appl. Surf. Sci. Adv.* **2021**, *6*, 100173.
(15) Wang, C.; Cai, X.; Chen, Y.; Cheng, Z.; Luo, X.; Mo, S.; Jia, L.; Lin, P.; Yang, Z. Improved hydrogen production from glycerol photoreforming over sol-gel derived TiO_2 coupled with metal oxides. *Chem. Eng. J.* **2017**, *317*, 522−532.
(16) Ullah, A.; Ullah, S.; Khan, M. Q.; Hashmi, M.; Nam, P. D.; Kato, Y.; Tamada, Y.; Kim, I. S. Manuka honey incorporated cellulose acetate nanofibrous mats: fabrication and in vitro evaluation as a potential wound dressing. *Int. J. Biol. Macromol.* **2020**, *155*, 479−489.
(17) Phan, D.-N.; Khan, M. Q.; Nguyen, N.-T.; Phan, T.-T.; Ullah, A.; Khatri, M.; Kien, N. N.; Kim, I.-S. A review on the fabrication of several carbohydrate polymers into nanofibrous structures using electrospinning for removal of metal ions and dyes. *Carbohydr. Polym.* **2021**, *252*, 117175.
(18) Phan, D.-N.; Lee, H.; Huang, B.; Mukai, Y.; Kim, I.-S. Fabrication of electrospun chitosan/cellulose nanofibers having adsorption property with enhanced mechanical property. *Cellulose* **2019**, *26*, 1781−1793.
(19) Phan, D.-N.; Khan, M. Q.; Nguyen, V.-C.; Vu-Manh, H.; Dao, A.-T.; Thanh Thao, P.; Nguyen, N.-M.; Le, V.-T.; Ullah, A.; Khatri, M.; et al. Investigation of mechanical, chemical, and antibacterial properties of electrospun cellulose-based scaffolds containing orange essential oil and silver nanoparticles. *Polymers* **2021**, *14* (1), 85.
(20) Barhoum, A.; Pal, K.; Rahier, H.; Uludag, H.; Kim, I. S.; Bechelany, M. Nanofibers as new-generation materials: from spinning and nano-spinning fabrication techniques to emerging applications. *Appl. Mater. Today* **2019**, *17*, 1−35.
(21) Zhang, K.; Li, Z.; Kang, W.; Deng, N.; Yan, J.; Ju, J.; Liu, Y.; Cheng, B. Preparation and characterization of tree-like cellulose nanofiber membranes via the electrospinning method. *Carbohydr. Polym.* **2018**, *183*, 62−69.
(22) Wu, H.; Inaba, T.; Wang, Z.-M.; Endo, T. Photocatalytic TiO_2@CS-embedded cellulose nanofiber mixed matrix membrane. *Appl. Catal., B* **2020**, *276*, 119111.
(23) Zhang, H.; Liu, B. Preparation, characterization, and photocatalytic properties of self-standing pure and Cu-doped TiO_2 nanobelt membranes. *ACS Omega* **2021**, *6* (7), 4534−4541.
(24) Sofi, H. S.; Akram, T.; Shabir, N.; Vasita, R.; Jadhav, A. H.; Sheikh, F. A. Regenerated cellulose nanofibers from cellulose acetate: incorporating hydroxyapatite (HAp) and silver (Ag) nanoparticles (NPs), as a scaffold for tissue engineering applications. *Mater. Sci. Eng. C* **2021**, *118*, 111547.
(25) Kudo, A.; Niishiro, R.; Iwase, A.; Kato, H. Effects of doping of metal cations on morphology, activity, and visible light response of photocatalysts. *Chem. Phys.* **2007**, *339* (1−3), 104−110.
(26) Thongpool, V.; Phunpueok, A.; Jaiyen, S.; Sornkwan, T. Synthesis and photocatalytic activity of copper and nitrogen Co-doped titanium dioxide nanoparticles. *Results Phys.* **2020**, *16*, 102948.
(27) Avilés-García, O.; Espino-Valencia, J.; Romero, R.; Rico-Cerda, J. L.; Arroyo-Albiter, M.; Natividad, R. W and Mo doped TiO_2: synthesis, characterization and photocatalytic activity. *Fuel* **2017**, *198*, 31−41.
(28) Karuppasamy, P.; Nisha, N. R. N.; Pugazhendhi, A.; Kandasamy, S.; Pitchaimuthu, S. An investigation of transition metal doped TiO_2 photocatalysts for the enhanced photocatalytic decoloration of methylene blue dye under visible light irradiation. *J. Environ. Chem. Eng.* **2021**, *9* (4), 105254.
(29) Meenatchisundaram, N.; Chellamuthu, J.; Jeyaraman, A. R.; Arjunan, N.; Muthuramalingam, J. B.; Karuppuchamy, S. Biosynthesized TiO_2 nanoparticles an efficient biogenic material for photocatalytic and antibacterial applications. *Energy Environ.* **2022**, *33* (2), 377−398.
(30) Wang, N.; Chen, J.; Wang, J.; Feng, J.; Yan, W. Removal of methylene blue by polyaniline/TiO_2 hydrate: adsorption kinetic, isotherm and mechanism studies. *Powder Technol.* **2019**, *347*, 93−102.
(31) Tran, H.; Wang, Y.-F.; You, S.-J.; Chao, H.-P. Insights into the mechanism of cationic dye adsorption on activated charcoal: the importance of π-π interactions. *Process Saf. Environ. Prot.* **2017**, *107*, 168−180.
(32) (a) Bansal, J.; Swami, S. K.; Tabassum, R.; Sharma, S. N.; Hafiz, A. K. Encapsulation of Cu-doped TiO_2 nanocomposites with the understanding of weak photocatalytic properties for sunscreen applications. *J. Dispersion Sci. Technol.* **2022**, *43* (3), 364−374. (b) Carvalho, H. W.; Batista, A. P.; Hammer, P.; Ramalho, T. C. Photocatalytic degradation of methylene blue by TiO_2-Cu thin films: theoretical and experimental study. *J. Hazard. Mater.* **2010**, *184* (1−3), 273−280.
(33) Ambikakumari Sanalkumar, K. U.; Yang, E.-H. Self-cleaning performance of nano-TiO_2 modified metakaolin-based geopolymers. *Cement Concr. Compos.* **2021**, *115*, 103847.

https://doi.org/10.1021/acsomega.4c00656
ACS Omega 2024, 9, 22734−22743